Springer

KSME

Journal of Mechanical Science and Technology 33 (9) (2019) 4281~4289
www.springerlink.com/content/1738-494x(Print)/1976-3824(Online)
DOI 10.1007/s12206-019-0824-x

Creating round focused micro-jets from rectangular nozzles †

Venkatesh Inguva[1,*], Rita Graceffa[2], Joachim Schulz[2], Osman Bilsel[3] and Blair J. Perot[1]

[1]*University of Massachusetts Amherst, Massachusetts, USA*
[2]*European XFEL, Hamburg, Germany*
[3]*University of Massachusetts Medical School, Massachusetts, USA*

(Manuscript Received January 21, 2019; Revised April 10, 2019; Accepted June 3, 2019)

Abstract

A focused jet is an axisymmetric jet of liquid surrounded by an outer coaxial gas jet. The gas jet is typically used to compress the liquid jet in the radial direction thereby focusing it. At microscales, it is difficult to manufacture micro-scale delivery nozzles (needles) and to consistently align and axially position the liquid and the gas needles. However, it is very easy, using standard etching technologies to make precise and repeatable rectangular nozzle designs. This work will therefore explore the geometric and fluid dynamics constraints that allow one to design rectangular nozzles that produce round coaxial micro-jets of liquid and gas. Because of the small scales, the fluid dynamics of the focusing jet is unusual, and this work demonstrates that the liquid jet is best focused by shear stretching and not via gas compression. This paper shows that sheet jetting occurs when the Reynolds number of the gas is too high. Dripping occurs when the Weber number of the liquid is too low. The desired round jet occurs by balancing Weber number of the liquid jet and Reynolds number of the gas such that surface tension at the interface holds the water jet round while the acceleration of the water jet due to shear at the interface from fast-moving air causes the liquid jet cross-sectional area to decrease. The goal of this initial paper is to demonstrate that a parameter region exists where this flow behavior is possible.

Keywords: Computational fluid dynamics; Microjets; X-ray free electron laser; Weber number; Reynolds number; Round jets; Rectangular geometry

1. Introduction

Micron scale liquid streams are used in industrial applications such as inkjet printers, 3D extrusion printers and spray nozzles. Inkjet printers are split into continuous inkjets and drop-on-demand inkjets [1] where ink droplets are created and deposited onto a surface. Inkjet printers usually operate [2] with Reynolds number in the range of 0.3 to 1 and Weber number in the range of 4 to 400. Droplets created are usually between 20 μm and 50 μm in diameter. 3D extrusion printers typically use nozzles with diameters of 400 μm [3] and create liquid jets that quickly solidify upon extrusion. A parametric study on the filament flow regime after it exits the extrusion nozzle does not exist. Spray nozzles typically have orifice diameters around 250 μm [4]. The jet operates [5] at Reynolds numbers around 1000 and Weber numbers at 80 for shear breakup while making sure Ohnesorge number is less than 0.01.

Experimental research applications of micron scale liquid streams are commonly seen in serial crystallography [6] using an X-ray free electron laser (XFEL) or synchrotron sources. The most commonly used type of device in these research applications is the gas dynamic virtual nozzle (GDVN) [7]. This device uses a stream of gas surrounding a liquid jet to focus the liquid jet into a smaller diameter. Jetting occurs at a Weber number greater than 3 for the liquid jet. The liquid jet cannot usually start at the desired final smaller diameter for various mechanical reasons, such as channel clogging by embedded crystals, or due to the excessive pressure drops that very small tubes cause. The greatest difficulty with GDVN (coaxial gas/liquid jets) is that slight misalignment from the center axis of the concentric tubes containing gas and liquid can dramatically interfere with the operation of the GDVN. Another approach proposed to achieve focused micron scale jets is electrospinning [8]. This method accelerates a polymeric solution in an electric field to create a micron scale jet. This technique has been successfully used to reduce the flow rate required compared to the GDVN and thereby reduce sample consumption in crystallography studies using an XFEL [9]. A parametric study [10] on the focusing aspect of the GDVN indicates that it is the pressure difference due to the gas flow that is the main physics in focusing the liquid jet in a GDVN.

Creating micron scale liquid streams in the form of jets, drops or sprays is of significant interest in industrial and aca-

*Corresponding author. Tel.: +1 413 545 3925, Fax.: +1 413 545 1027
E-mail address: vinguva@alumni.purdue.edu
† Recommended by Associate Editor Donghyun You

demic applications. Three dimensionless parameters [11] play an important role in determining the flow regime of the liquid. These three parameters are the Weber, Reynolds, and Ohnesorge numbers. The Weber and Reynolds numbers are the parameters with which this work will consider to be primary and the Ohnesorge number is simply the ratio of the square root of the Weber number and the Reynolds number. By varying the primary parameters where a liquid stream is present, it is possible to change the flow regime of the liquid stream.

Two studies have been conducted on developing microfluidic devices that can focus micro-jets. Both studies used computational fluid dynamics (CFD). The first study [9] used the OpenFOAM solver interMixingFoam to model the focusing of a liquid jet in a GDVN along with mixing within the liquid phase. This study was interested in modeling the classic axisymmetric nozzle design. The second study [12] by Trebbin et al. used Comsol's multiphase solver to model a rectangular geometry device to create a round jet. However, that work did not propose any parameters for the operation of such a rectangular geometry device nor did it document the geometry optimization process to achieve round jets using rectangular geometry, which this paper does. More studies related to microjets are done by Rosello et al. [13] pertaining to nozzle shape influence on micro inkjets, Ngo et al. [14] pertaining the effects of viscosity and junction angle on droplet formation in microfluidic junctions and Carroll et al. [15] pertaining to droplet detachment in high speed gaseous microflows.

This paper uses the OpenFOAM interFoam solver [16] to explore the geometric and flow parameters necessary to achieve round focused liquid jets using rectangular nozzle geometry. This work does not delineate the entire operating parameter space, but does explore a few different operating conditions and nozzle designs that create different flow regimes such as round jetting, planar sprays, and dripping. The main advantage of using rectangular geometry for microfluidic devices is they can be easily manufactured with high precision using a laser etching process [17].

2. Methods

This work uses ICEM CFD [18] for meshing, the open source toolbox OpenFOAM's [16] solver interFoam to compute the flow and paraview [19] for post-processing of simulation results. Hexahedral elements aided by coarse scale domain blocking was chosen to discretize the full simulation domain. Control over the mesh resolution in critical zones is provided by the blocking step. The solver settings for interFoam as are follows. Time stepping was done by an implicit Euler scheme. Gradient and divergence schemes are linear. Laplacian and surface normal gradient schemes are linear corrected. Interpolation schemes are linear. All matrix inversions have their tolerances set to 1E-6 or smaller. The supercomputer used is Stampede II at the Texas Advanced Computing Center (TACC) [20]. The various simulation domains were discretized with an average of 8 million cells and each computed using 256 cores distributed on 4 nodes consisting of 4 Intel Xeon Phi 7250 Knights Landing processors. Post-processing was carried out on a local computer consisting of 32 GB of RAM and an Intel Skylake i7-6700k processor. All simulations were run for at least 0.0004 s simulation time and no longer than 0.0005 s. This was to save on computing hours which the total usage for this paper was around 500000 core hours.

2.1 InterFoam formulation

The interFoam solver computes the solution to the incompressible multiphase Navier-Stokes equations. The incompressible Navier-Stokes equations [21, 22] are given by Eqs. (1) (mass) and (2) (momentum). Gravity is neglected in the simulations. The volume fraction transport equation [21] indicating the gas ($\alpha = 0$) and the liquid ($\alpha = 1$) regions is given by Eq. (3).

$$\frac{\partial U_i}{\partial x_i} = 0 . \tag{1}$$

$$\frac{\partial \rho U_i}{\partial t} + \frac{\partial \rho U_i U_j}{\partial x_i} = -\frac{\partial p}{\partial x_i} + \frac{\partial}{\partial x_i}\left(2\left(\mu + \mu_t\right)S_{ij}\right) + \sigma\kappa\frac{\partial \alpha}{\partial x_i} . \tag{2}$$

$$\frac{\partial \alpha}{\partial t} + \frac{\partial \alpha U_i}{\partial x_i} + \frac{\partial}{\partial x_i}\left(\alpha\left(1-\alpha\right)U_i^r\right) = 0 . \tag{3}$$

The variables are defined as below. U is velocity. ρ is the density. μ is the dynamic viscosity. μ_t is the turbulent viscosity. S_{ij} is the strain-rate tensor. σ is the surface tension. κ is the interface curvature. The term containing U_i^r is an artificial compressibility term to keep the interface sharp and U_i^r is modelled as in Ref. [21]. α is the volume fraction where 0 indicates gas phase and 1 indicates liquid phase.

To compute a generic fluid property Θ, (such as μ or ρ) the averaging is given by

$$\Theta = \alpha\Theta_{liquid} + (1-\alpha)\Theta_{gas} . \tag{4}$$

2.2 k-ω SST turbulence model

To model the turbulent viscosity, μ_t in Eq. (2), the $k-\omega$ shear stress transport (SST) model [23] is used. It is given by Eqs. (5)-(7).

$$\frac{\partial k}{\partial t} + U_j\frac{\partial k}{\partial x_j} = P_k - \beta^* k\omega + \frac{\partial}{\partial x_j}\left[\left(\nu + \frac{\sigma_k\mu_t}{\rho}\right)\frac{\partial k}{\partial x_j}\right] . \tag{5}$$

$$\frac{\partial \omega}{\partial t} + \left\langle U_j\right\rangle\frac{\partial \omega}{\partial x_j} = \alpha S_{ij}^2 - \beta\omega^2 + \frac{\partial}{\partial x_j}\left[\left(\frac{\mu}{\rho} + \frac{\sigma_\omega\mu_t}{\rho}\right)\frac{\partial \omega}{\partial x_j}\right] + 2(1-F_1)\sigma_{\omega 2}\frac{1}{\omega}\frac{\partial \omega}{\partial x_i}\frac{\partial k}{\partial x_i} . \tag{6}$$

$$\mu_t = \frac{\rho\alpha_1 k}{\max(\alpha_1\omega, SF_2)} . \tag{7}$$

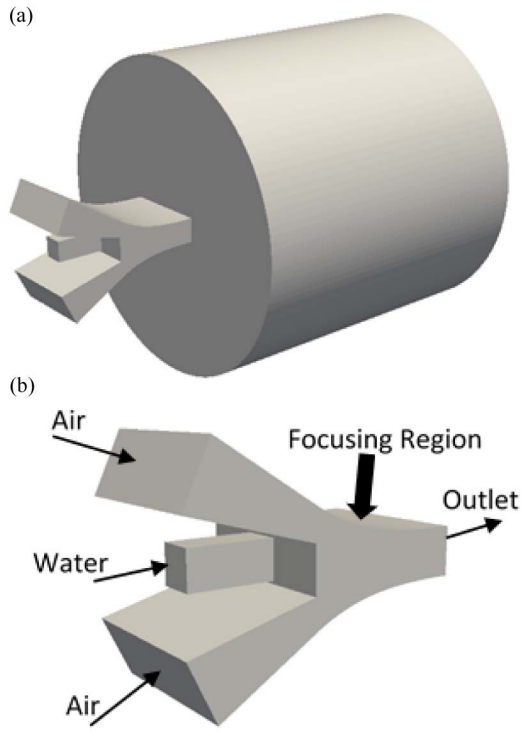

Fig. 1. Geometry and flow configuration of a focusing nozzle: (a) Nozzle with exhaust plenum; (b) nozzle with flow configuration.

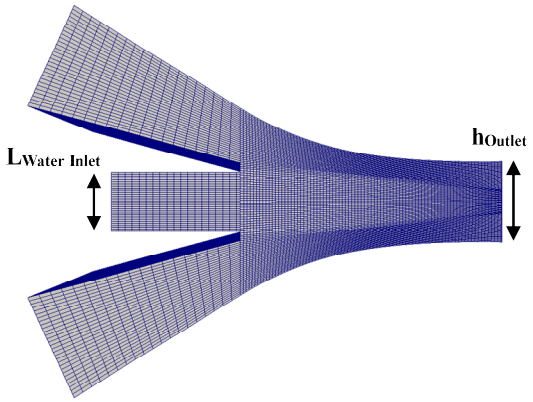

Fig. 2. Mesh of geometry in Fig. 1 showing resolution.

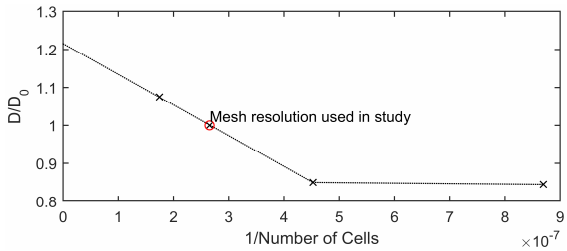

Fig. 3. Mesh resolution study of nozzle 1. D/D_0 is normalized jet diameter. Note: X-axis is 1 divided by the number of cells. 1/number of cell = 0 indicates mesh of infinite resolution.

Eq. (5) models k, the turbulent kinetic energy, and Eq. (6) models ω, the specific rate of dissipation. Eq. (7) determines the turbulent viscosity μ_t from those two scales. P_k is the turbulence production term. $\alpha_1, \beta^*, \beta, \sigma_k, \sigma_\omega, \sigma_{\omega 2}$ are tuning constants. F_1 and F_2 are blending functions, all found in Ref. [20]. This model was selected because it was found to be active in the microscale [24].

2.3 Flow configuration, boundaries, mesh and mesh resolution study

Fig. 1 shows the geometry of one of the focusing nozzles. A detailed drawing of the optimized design is given at the end of the results section. All simulations in this paper have the gas phase as air and the liquid phase as water when setting property values, but the materials used do not actually matter, as only the dimensionless parameters like Weber number and Reynolds number dictate the dynamics. In Fig. 1, the gas (air) enters the top and bottom inlets at a fixed speed. The liquid (water) enters the central channel at a slower (than the gas) fixed speed. Fig. 1(a) shows the general geometry for the focusing nozzle along with the plenum into which the gas and liquid exhausts into. The plenum, a large meshed region attached to the outlet in Fig. 1(a), has zero gradient boundary conditions. All the walls of the device in Fig. 1(b) have no-slip boundary conditions. Fig. 2 shows the mesh on the surface of the geometry. All the simulations have similar mesh resolution to Fig. 2. The geometry in Fig. 1 is designated as nozzle 1. The diameter of the resultant jet of all different simulations where round jetting occurs is given in Table 1.

A mesh resolution study is done on nozzle 1 to determine the error in resultant jet diameter due to grid dependence. Fig. 3 shows the normalized resultant just diameter normalized with D_0 which is the resultant jet diameter using the mesh resolution of Fig. 2 which contains 3770979 cells. As seen in Fig. 3, when the number of cells reaches infinity, the resultant jet is 1.2156 times larger than the jet diameter predicted by using the mesh resolution of Fig. 2 indicating an error of 17.7 % due to grid dependence in this study. The change in jet diameter due to mesh is linear up to the point when the mesh is too coarse to correctly advect the jet. The grid resolution of 3770979 cells is chosen as it is possible to practically model geometry to achieve round jets from rectangular geometry using a supercomputer. Due to the discontinuity in the flow inherent to multiphase simulations, the resultant jet diameter will generally tend to be mesh dependent for all mesh resolutions.

3. Results

The Weber number of the water (based on the length of a side of the square water inlet, $L_{WaterInlet}$ in Fig. 2, and the uniform inlet velocity of the water) and the Reynolds number (based on the height of the outlet, h_{outlet} in Fig. 2, and the average velocity of the air at the outlet) are also given in Table 1. The absolute mass flow rates of air and water are further fur-

Table 1. Jet diameter, Reynolds and Weber number and mass flow rates for air and water for nozzles simulated where round jetting occurs.

Nozzle	D (μm)	Re_{air}	Wb_{water}	$\dot{m}_{air}$ *10^{-6} (kg/s)	$\dot{m}_{water}$ *10^{-5} (kg/s)
1	55	680	0.86	5.40	1.17
2	39	680	0.86	5.40	1.17
3	19	680	1.2	5.40	0.324
4	14	680	1.2	5.40	0.324

nished in Table 1 also.

The Weber number in this study is defined as follows by Eq. (8) where $U_{WaterInlet}$ is the boundary velocity condition specified in each simulation.

$$Wb_{water} = \frac{\rho_{water} U^2_{waterinlet} L_{waterinlet}}{\sigma}. \quad (8)$$

The Reynolds number in this study is defined as follows by Eq. (9) where $U_{Avg,Outlet}$ is the average velocity of air exiting the outlet.

$$\mathrm{Re}_{air} = \frac{\rho_{air} U_{avg.outlet} h_{outlet}}{\mu_{air}}. \quad (9)$$

The fundamental physics behind the operation of these types of nozzles is that Weber number should be low enough for the surface tension to make the jet round after it exits the water channel but high enough for the liquid jet to be in the jetting regime. The air surrounding the jet imposes shear stress at the air-water interface causing the jet to accelerate. This acceleration of the liquid by the gas is what causes the jet to decrease its diameter (due to conservation of mass) causing the focusing. It is tempting to think that the gas jets are impinging (at an angle) on the liquid jet and therefore compressing ("squeezing") the liquid jet. But this effect is very small compared to the shear acceleration. Any appreciable compression will make the liquid jet flatten into a sheet and break apart. Fig. 4 shows the operating parameter space explored and geometry optimization process used to design the rectangular focusing nozzle presented in Fig. 5.

3.1 Nozzle 1 at Wb_{water} = 0.86 and Re_{air} = 680

In nozzle 1, the dimensions of the water inlet are 125 μm by 125 μm wide. Fig. 4(a) shows the resultant focused jet formed at Wb_{water} = 0.86 and Re_{air} = 680 along with the speed of the jet. The resultant jet diameter at the outlet is 55 μm. This is a reduction in area of 84.8 %. The speed of the jet increases from 0.69 m/s to 4.56 m/s. However, it is desired to decrease the resultant jet diameter and increase its speed further. As such, the Reynolds number of the air is increased by double to 1360 to increase the amount of shear at the air-water interface allowing for more acceleration.

3.2 Nozzle 1 at Wb_{water} = 0.86 and Re_{air} = 1360

Increasing the Reynolds number to 1360 increases the inertial effects of the air (kinetic energy and stagnation pressure) by 4 times. As seen in Fig. 4(b) this increase in inertia of the air causes the resultant jet to compress ("squeeze" due to excessive air pressure) and lose its round shape. The increased shear stress due to the increased air speed causes the water bulb formed to shed in thin streams. This simulation shows that the Reynolds numbers of the air should not be so high as to cause compression, and a lower Reynolds number of 680 (Sec. 3.1) is actually better able to focus the jet while still keeping it round.

3.3 Nozzle 2 at Wb_{water} = 0.86 and Re_{air} = 680

In the next geometry iteration, nozzle 2 shown in Fig. 4(c), the angle of the air inlets is reduced to decrease the normal to the flow direction inertia imparted to the water jet. This design reduces the squeezing effect on the water jet away from its round shape. Also, the length of the focusing region is increased to allow the air to shear the air-water interface for a longer distance resulting in more shear acceleration. This results in the velocity of the jet increasing to 8.7 m/s. The diameter of the focused jet is 39 μm indicating that the increase in length of the focusing region allowed the jet to accelerate more and decrease its diameter further. This is a 92.4 % reduction in area. Fig. 4(c) also shows the jet swaying to the right, this is due to the jet start-up vortex that forms in the plenum and with enough simulation time, that vortex will wash out and the jet will become straight. This is an expectation based on the jets from the other nozzle designs being mostly straight where stable jetting occurs. We have not confirmed this expectation due to the high computing cost of these types of simulations.

3.4 Nozzle 2 at Wb_{water} = 0.86 and Re_{air} = 1360

To check if the decrease in air inlet angle allows higher inlet speeds, the Reynolds number of the air is increased to 1360 again like in Sec. 3.2. Fig. 4(d) shows the resultant jet. As seen, the round jet again starts to squeeze flat like in the case of Sec. 3.2. Given enough simulation time, it is likely the jet would look similar to Fig. 4(b). The round jet seen ahead of the flat sheet comes from the simulation being initialized from the case of Sec. 3.3 but not being run long enough to allow the round jet to exit the nozzle entirely. This case shows that there is a limit on the Reynolds number of the air such that not too much inertia is imparted onto the water jet allowing it to maintain its round shape. Lowering the angle did not allow a significant (twice the Reynolds number for the air) increase, but probably would allow a slightly higher Reynolds number for the air than 680.

3.5 Nozzle 3 at Wb_{water} = 1 and Re_{air} = 680

Nozzles 1 and 2 have the water inlet at 125 μm by 125 μm

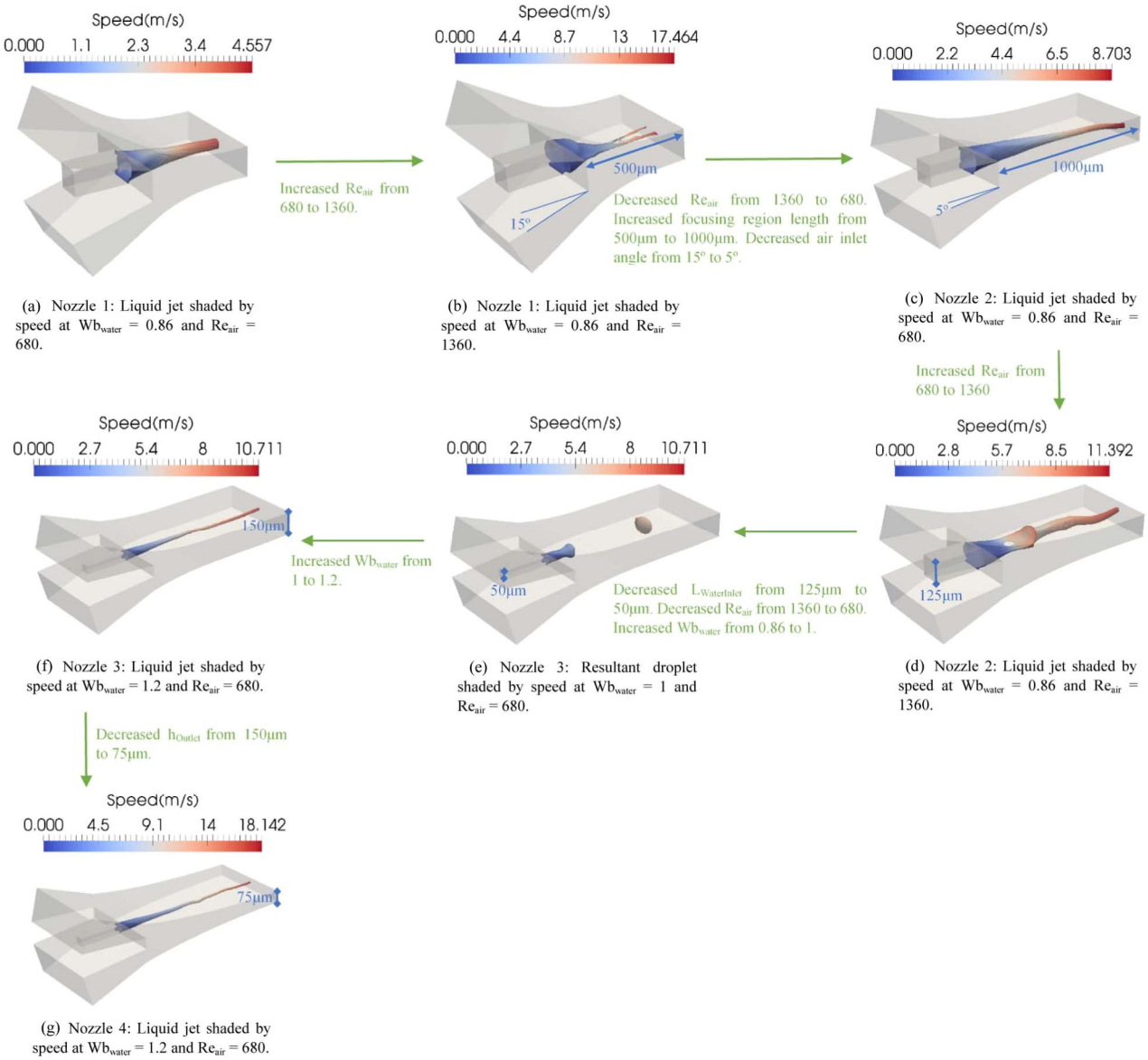

(a) Nozzle 1: Liquid jet shaded by speed at Wb_{water} = 0.86 and Re_{air} = 680.

(b) Nozzle 1: Liquid jet shaded by speed at Wb_{water} = 0.86 and Re_{air} = 1360.

(c) Nozzle 2: Liquid jet shaded by speed at Wb_{water} = 0.86 and Re_{air} = 680.

(d) Nozzle 2: Liquid jet shaded by speed at Wb_{water} = 0.86 and Re_{air} = 1360.

(e) Nozzle 3: Resultant droplet shaded by speed at Wb_{water} = 1 and Re_{air} = 680.

(f) Nozzle 3: Liquid jet shaded by speed at Wb_{water} = 1.2 and Re_{air} = 680.

(g) Nozzle 4: Liquid jet shaded by speed at Wb_{water} = 1.2 and Re_{air} = 680.

Fig. 4. Flowchart showing geometry and operating parameter optimization with key geometry changes documented.

in dimension. Nozzle 3 and its resultant jet is shown in Fig. 4(e). Nozzle 3 has the water inlet at 50 µm by 50 µm. This is to reduce the initial area of the jet exiting the water inlet so it would be able to focus to a smaller diameter in the focusing region. However, from Fig. 4(e), it appears that the very slightly higher Weber number of 1 is not able (for this geometry) to put the jet into the jetting regime and it is instead dripping. This suggests some geometry dependence along with Weber number in classifying the flow regime of this class of focusing nozzles.

3.6 Nozzle 3 at Wb_{water} = 1.2 and Re_{air} = 680

Increasing the Weber number to 1.2 puts nozzle 3 jet into the jetting regime as seen in Fig. 4(f). The diameter of the jet at the outlet is now 19 µm and the area reduction is 88.7 %. The speed of the water jet at the outlet is 10.7 m/s. Decreasing the area of the of the inlet allowed the resultant focused jet to decrease its diameter from 39 µm to 19 µm. This is a significant improvement with the same air inlet speed and Reynolds number.

3.7 Nozzle 4 at Wb_{water} = 1.2 and Re_{air} = 680

So far, no geometry optimization has been done on the downstream focusing region of the nozzle. It has only been extended to increase the length upon which air can shear the air-water interface. Nozzles 1 through 3 have the outlet height at 150 µm. In nozzle 4, shown in Fig. 4(g) the height of the outlet is reduced to 75 µm. This causes the gas to continue

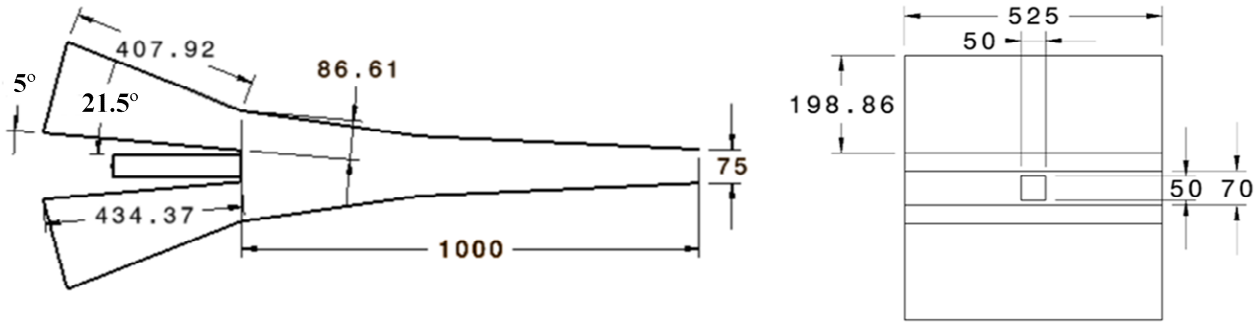

Fig. 5. Detailed drawing of nozzle 4 indicating important dimensions. Units are μm where no units are shown.

accelerating even as the liquid attempts to accelerate to the gas speed. Hence the speed of the air in this design is faster at the exit of the focusing region (at the very end of the nozzle). This increase in speed allows more shear to be exerted on the air-water interface allowing the jet to be focused and accelerated even further than its predecessor, nozzle 3. The diameter of the resultant jet is 14 μm. This is an area reduction of 93.8 %. The speed of the jet at the outlet is 18.1 m/s. It should be noted that bringing the wall closer to the water jet appears to induce some instability into the water jet. Hence, there is a trade-off between the ability to focus and the stability of the water jet. A detailed drawing of nozzle 4 is shown in Fig. 5.

4. Discussion

To further understand the physics of how focusing occurs, the nozzles at operating conditions which create round jets are further studied to determine which fluid physics play a crucial role.

4.1 Speed profiles around jets

Speed profiles at the outlet for nozzles 1 to 4 where round jets are created are shown in Fig. 6. Care was taken to ensure that maximum speed in these nozzles are less than 105 m/s or Mach number less than 0.3. At Ma = 0.3, the isentropic flow relation [25] for ρ/ρ_0 is 0.956 meaning there is a 4.4 % error in the velocity computed from the incompressible assumption. In the case of nozzle 4, the geometry change increased the maximum speed to 180.8 m/s or a Mach number of 0.52. The isentropic flow relation for ρ/ρ_0 at Ma = 0.52 is 0.877 meaning there are small compressibility affects in the air that we are not computing (the air is actually slightly slower and denser than computed). The compressible formulation of interFoam used in the OpenFOAM solver compressibleInterFoam proved to be too stiff and unstable to solve this type of flow problem and hence was not used. The incompressible formulation still provides useful information about the flow.

From Fig. 6, the boundary layer surrounding the jets created by air slowing down to the speed of the jet is observed. In Figs. 6(a) and (d), it can be seen that the boundary layer on the top/bottom of the water jet is affected by the top/bottom nozzle walls and results in jets that are not perfectly round. However, this slight distortion is rapidly corrected by surface tension once the liquid jet enters the plenum where the experiments occur. In Figs. 6(b) and (c), the boundary layer is well formed and the jets are already fully round. Fig. 6(b) has a jet that is not well centered due to the start-up plenum vortex and the short time duration of this run. It still gives a good indication of the liquid jet cross section and the gas boundary layer that accelerates the liquid jet.

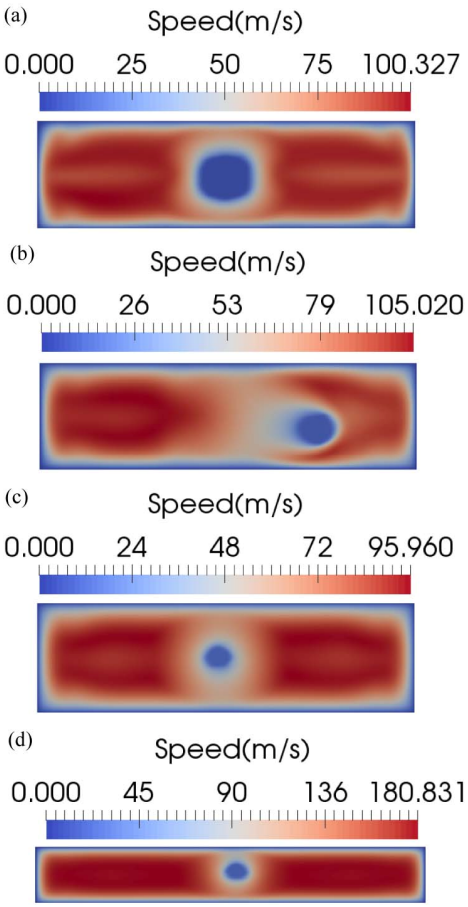

Fig. 6. Speed profiles at outlet. Note slow speed in the centers indicate the position and speed of the water jet: (a) Nozzle 1; (b) nozzle 2; (c) nozzle 3; (d) nozzle 4.

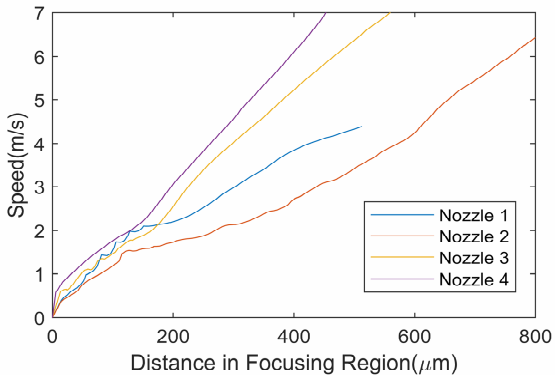

Fig. 7. Speed of air-water interface in the focusing region of all nozzles.

4.2 Flow development of liquid jet

The gas boundary layer also has an impact on the flow profile inside the liquid jet. The speed of the air-water interface for all nozzles where round jetting occurs is studied further. Fig. 7 shows the speed plotted against the distance in the focusing region. The starting plane, 0 μm, is indicated in Fig. 8. As seen in Fig. 7, the speed of the interface for all nozzle initially increases at a particular gradient, then at about 150 μm, the gradient changes.

To understand the reason for this change in gradient, the velocity profiles in liquid jet for all nozzles is studied in Fig. 8. As seen in Fig. 8, the flow initially exits the water inlet with the profile of that of a Poiseuille flow with the slowest speed at the interface of the liquid jets and the fastest speed at the center of the liquid jets. The flow in the liquid jets then begin an inversion process that occurs from 0 μm to about 150 μm in the focusing region of all the nozzles. Once the inversion process is complete, the fastest speed of the liquid jets is at the interface while the slowest speed is at the center of the liquid jets. This inversion process would explain the change in gradients of the interface speed in Fig. 7.

5. Conclusion

This paper shows the geometry optimization process for creating thin focused round micro-jets from rectangular nozzles. Rectangular nozzle geometry in microfluidics is preferable because it can be repeatedly manufactured with high precision using laser etching processes.

The important flow parameters were demonstrated via example to be the Weber number of the liquid jet and the Reynolds number of the gas jet. The weber number of the liquid jet should be near to 1. Surface tension is crucial to make the jet round. A Reynolds number for the gas of 680 is sufficient to create enough shear via a boundary layer at the gas-liquid interface to drag to the liquid jet down the focusing region and causing it to accelerate significantly. This reduces the liquid jets diameter (due to incompressibility, $A_1U_1 = A_2U_2$). Too high a Reynolds number for the air imparts too much radial inertia to the water jet causing it to flatten and lose its round

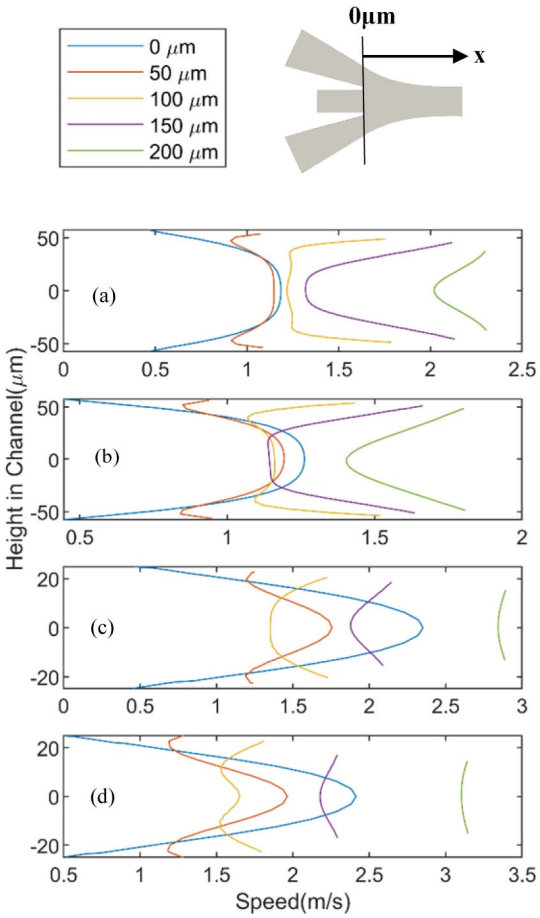

Fig. 8. Speed profile inside water jet of nozzles as it travels down the focusing region: (a) Nozzle 1; (b) nozzle 2; (c) nozzle 3; (d) nozzle 4.

shape. This can be somewhat ameliorated by reducing the incoming angle of the air jet.

The geometry optimization process indicated that an area reduction of the liquid jet on the order of 95 % is quite possible. Longer nozzles (with more total acceleration) can increase the area reduction further. We showed that it is also possible to further accelerate the air, in order to increase the acceleration of the liquid jet. The diameter of the final focused jet is inversely proportional to the length of the focusing region and the magnitude of the average acceleration over that length.

The contact angle between the liquid and the walls of the nozzle, as a result of material properties of the nozzle, will only have an effect at one region in this type of nozzle which is the edges between the water inlet and the focusing region. This will affect the Poiseuille flow profile of the jet as it exits the water outlet. We speculate this effect to have a delaying effect on the development of the focused liquid jet as the liquid jet will exit into the focusing region slightly wider than what our simulations predict. However, the overall focusing aspect of the nozzle will not be impacted by the contact angle of the material.

Bringing the boundary walls of the focusing region closer to

the liquid jet causes the development of the gas boundary layer to become more unsteady due to higher air speed between the liquid jet and the wall and higher shear as a result. A high resolution LES study of the gas interacting with the liquid jet is required to fully visualize and understand the effect the unsteady gas boundary layer has on the liquid jet.

The main fluid physics of this type of coaxial gas/liquid jet is using surface tension to hold the jet round and using shear form the gas boundary layer at the gas-liquid interface to accelerate the jet thereby causing area reduction or focusing of the liquid jet.

Acknowledgments

We would like to thank NSF for funding this work. The work is supported by NSF IDBR Award No. 1353942. We acknowledge the Texas Advanced Computing Center (TACC) at The University of Texas at Austin for providing HPC, visualization and database resources that have contributed to the research results reported within this paper.

Nomenclature

U	: Velocity
ρ	: Density of fluid
μ	: Viscosity of fluid
α	: Volume fraction of liquid phase
Θ	: Material property of fluid
k	: Turbulent kinetic energy
ω	: Specific rate of turbulence dissipation
μ_T	: Turbulent viscosity
$L_{WaterInlet}$	: Length of side of square water inlet
h_{Outlet}	: Height of outlet of nozzle
Wb_{Water}	: Weber number of water at the water inlet
Re_{Air}	: Reynolds number of air at nozzle outlet
$\dot{m}_{air}$	: Mass flowrate of air in nozzle
$\dot{m}_{water}$	: Mass flowrate of water in nozzle
D	: Diameter of liquid jet at outlet
D_0	: Diameter of liquid jet at mesh resolution specified

References

[1] B. de Gans, P. C. Duineveld and U. S. Schubert, Inkjet printing of polymers: State of the art and future developments, *Advanced Materials,* 16 (3) (2004) 203-213.

[2] B. Derby, Inkjet printing of functional and structural materials: Fluid property requirements, feature stability, and resolution, *Annual Review of Materials Research,* 40 (2010) 395-414.

[3] O. Carneiro, A. Silva and R. Gomes, Fused deposition modeling with polypropylene, *Materials & Design,* 83 (2015) 768-776.

[4] S. Som, A. I. Ramirez and D. E. Longman, Effect of nozzle orifice geometry on spray, combustion, and emission characteristics under diesel engine conditions, *Fuel,* 90 (3) (2011) 1267-1276.

[5] G. Faeth, L. Hsiang and P. Wu, Structure and breakup properties of sprays, *International Journal of Multiphase Flow,* 21 (1995) 99-127.

[6] H. N. Chapman, P. Fromme and A. Barty, Femtosecond X-ray protein nanocrystallography, *Nature,* 470 (7332) (2011) 73.

[7] D. DePonte, U. Weierstall and K. Schmidt, Gas dynamic virtual nozzle for generation of microscopic droplet streams, *Journal of Physics D: Applied Physics,* 41 (19) (2008) 195505.

[8] S. V. Fridrikh, H. Y. Jian and M. P. Brenner, Controlling the fiber diameter during electrospinning, *Physical Review Letters,* 90 (14) (2003) 144502.

[9] D. Oberthuer, J. Knoška and M. O. Wiedorn, Double-flow focused liquid injector for efficient serial femtosecond crystallography, *Scientific Reports,* 7 (2017) 44628.

[10] A. M. Gañán-Calvo and J. M. Montanero, Revision of capillary cone-jet physics: Electrospray and flow focusing, *Physical Review E,* 79 (6) (2009) 066305.

[11] G. H. McKinley and M. Renardy, Wolfgang Von Ohnesorge, *Physics of Fluids,* 23 (12) (2011) 127101.

[12] M. Trebbin, K. Krüger and D. DePonte, Microfluidic liquid jet system with compatibility for atmospheric and high-vacuum conditions, *Lab on a Chip,* 14 (10) (2014) 1733-1745.

[13] M. Rosello, G. Maîtrejean and D. C. Roux, Influence of the nozzle shape on the breakup behavior of continuous ink jets, *Journal of Fluids Engineering,* 140 (3) (2018) 031202.

[14] I. Ngo, S. W. Joo and C. Byon, Effects of junction angle and viscosity ratio on droplet formation in microfluidic cross-junction, *Journal of Fluids Engineering,* 138 (5) (2016) 051202.

[15] B. Carroll and C. Hidrovo, Droplet detachment mechanism in a high-speed gaseous microflow, *Journal of Fluids Engineering,* 135 (7) (2013) 071206.

[16] H. Jasak, A. Jemcov and Z. Tukovic, OpenFOAM: A C library for complex physics simulations, *International Workshop on Coupled Method in Numerical Dynamics*, 1000 (2007) 1-20.

[17] Y. Bellouard, A. Said and M. Dugan, Fabrication of high-aspect ratio, micro-fluidic channels and tunnels using femtosecond laser pulses and chemical etching, *Optics Express,* 12 (10) (2004) 2120-2129.

[18] I. Ansys, Cfd, *ICEM CFD Theory Guide,* Ansys Inc. (2015).

[19] A. Henderson, J. Ahrens and C. Law, *The ParaView Guide*, Kitware Inc, Clifton Park, NY (2004).

[20] J. Towns, T. Cockerill and M. Dahan, XSEDE: Accelerating scientific discovery, *Computing in Science & Engineering,* 16 (5) (2014) 62-74.

[21] S. S. Deshpande, L. Anumolu and M. F. Trujillo, Evaluating the performance of the two-phase flow solver interfoam, *Computational Science & Discovery,* 5 (1) (2012) 014016.

[22] B. E. Larsen, D. R. Fuhrman and J. Roenby, Performance

of interfoam on the simulation of progressive waves, *Coastal Engineering Journal* (2019) 1-21.
[23] F. R. Menter, Two-equation Eddy-viscosity turbulence models for engineering applications, *AIAA Journal,* 32 (8) (1994) 1598-1605.
[24] V. Inguva, S. V. Kathuria and O. Bilsel, Computer design of microfluidic mixers for protein/RNA folding studies, *PloS One,* 13 (6) (2018) e0198534.
[25] J. D. Anderson, *Modern Compressible Flow: With Historical Perspective,* McGraw-Hill, 12 (1990).

Venkatesh Inguva is a Post-doctoral Researcher at Universität Paderborn. He completed his Ph.D. at the University of Massachusetts Amherst. His research involves the use of computational and experimental fluid dynamics to study flows in microchannels.

Rita Graceffa is a Scientific Officer at the Industrial Liaison Office at the European XFEL. She has experience in studying micro and milliseconds timescale kinetics initiated by fast mixing, by coupling microfluidics and x-rays.

Joachim Schulz is the Group Leader for Sample Environment & Characterization at the European XFEL. His research covers sample preparation and delivery methods for high repetition rate X-ray sources. Liquid jet sample delivery for serial femtosecond crystallography on protein crystals is a focus of this research.

Osman Bilsel is a Professor at University of Massachusetts Medical School. His research focuses on the mechanisms of protein folding and misfolding. He uses microfluidic mixers, time-resolved fluorescence and small-angle x-ray scattering to better understand early events in protein folding.

Blair J. Perot is a Professor at the University of Massachusetts Amherst. His research spans the full spectrum of using computers to solve fluid dynamics problems, from developing numerical techniques to applied research topics in microfluidics and wind turbines.